Colloids and Surfaces A: Physicochem. Eng. Aspects 466 (2015) 203–209

Contents lists available at ScienceDirect

Colloids and Surfaces A: Physicochemical and Engineering Aspects

journal homepage: www.elsevier.com/locate/colsurfa

Dynamic delamination of drying colloidal films: Warping and creep behavior

F. Giorgiutti-Dauphiné [1], L. Pauchard *

Univ Paris-Sud, CNRS, Lab FAST, Bat 502, Campus Univ, Orsay F-91405, France

HIGHLIGHTS

- We examine out-of-plane displacement of thin colloidal films during the drying process.
- Different behaviors can be distinguished from elastic to plastic then creep.
- Direct characterization of the mechanical properties is supported by measurements using indentation testing.

GRAPHICAL ABSTRACT

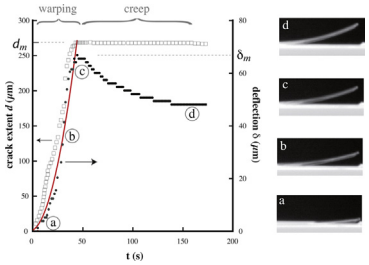

ARTICLE INFO

Article history:
Received 12 August 2014
Received in revised form
25 November 2014
Accepted 27 November 2014
Available online 8 December 2014

PACS:
47.57.J
62.20.M

Keywords:
Delamination
Drying
Colloidal suspension

ABSTRACT

During the consolidation of thin films, mechanical instabilities usually result from large mechanical stresses development. In particular morphologies of fractures and debonding reveal different behaviors of the materials. We report dynamic debonding induced by drying process of colloidal systems by direct measurements in a one-dimensional geometry. From the measurements of the film out-of-plane displacement, different behaviors can be distinguished from elastic to plastic then creep. The time evolution of the mechanical properties of colloidal films is in accordance with measurements using indentation testing as a response to an external force.

1. Introduction

Many industrial processes dedicated to material elaboration or to coating achievements, are based on the solidification of complex systems. In most common technological operations, the solidification is obtained through drying process of particulate materials. When the drying rate is high, large stresses appear and can lead to the formation of mechanical instabilities such as cracks providing a large variety of morphologies. These crack patterns can be commonly observed in nature, for soils in hot regions. Due to evaporation of water, the drying stress causes the clay to fracture into polygonal cells [1] (Fig. 1a). In practice, the control of these phenomena is crucial for all the coating technologies since they significantly alter the final film quality, and usually need to be avoided. There are two main kinds of drying cracks: the shrinkage cracks which propagate perpendicular to the film surface, and the peeling cracks which propagate parallel to the surface. The first type of cracks have been widely studied [2,3]. In the case of peeling cracks,

* Corresponding author. Tel.: +33 169158049; fax: +33 169158060.
E-mail addresses: fred@fast.u-psud.fr (F. Giorgiutti-Dauphiné), pauchard@fast.u-psud.fr (L. Pauchard).
[1] Tel.: +33 169158049; fax: +33 169158060.

http://dx.doi.org/10.1016/j.colsurfa.2014.11.061
0927-7757/

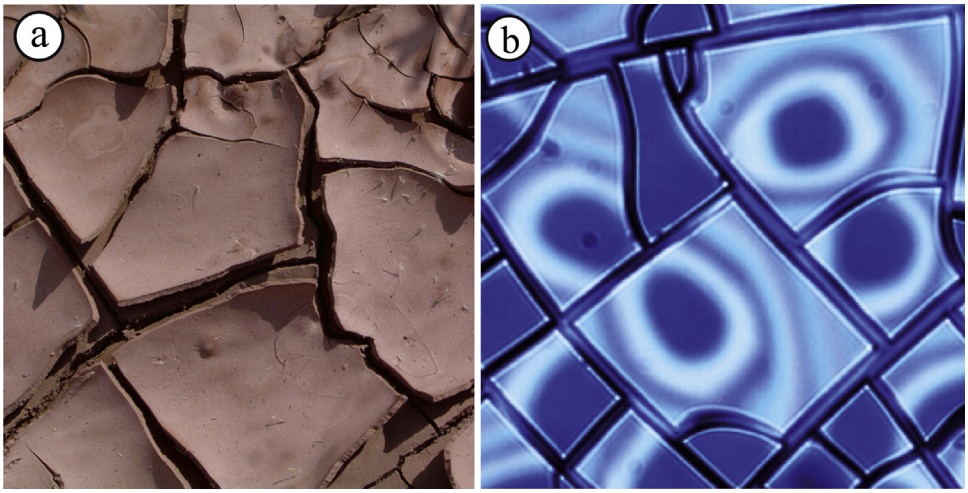

Fig. 1. (a) Warped mud, and desiccation polygons formed by the drying of clay. The largest polygons are approximately 30 cm in length (photograph courtesy of J.C. Géminard). (b) Colloidal film on a substrate. The channel cracks divide the transparent layer into polygons. The interference fringes indicate that the film also partially debonds from the substrate (image width =200 μm).

a model predicts a relationship between the thickness of the mud peel and the radius of curvature of the fragment [4,5]; this model is based on the differential contraction of layers. For practical reasons, only few works deal with the dynamics of the delamination crack front since it is not an easy task to follow the crack propagation. Moreover, the dynamics of the delamination of a film is a complex process since it is related to the evolution of the mechanical properties induced by the drying stress development. The drying film combines elastic, viscous and plastic behaviors. The final state of the dried film depends on these evolving properties. Indeed, channeling cracks, curl, warp, all induce deformations strongly related to the mechanical properties of the materials; also the resulting morphologies are characteristic processes of the time evolution of the material. This can be evidenced during the drying of paint layers or mud. Usually, peeling cracks start propagating from the corner and the borders of a fragment: the delamination is partial, e.g. the delamination process stops, fragments adhere to the underlayer only by a single region exhibiting a well defined surface area [6]. Then, the fragments become convex toward the drying side, lifting the corners off of the underlying layers (Fig. 1b). This evidences a plastic behavior of the system at the end of the evaporation process. Indeed, if it were purely elastic, the warped film should instantaneously relax back, and recover its initial flat state at the final stage.

In the following, we study the delamination process resulting from the drying of colloidal films in a well-controlled experiment, that exhibits no boundary conditions and presents a one-dimensional geometry. This is achieved by considering the drying of a thin film coating on a horizontal fiber. This particular geometry allows us a precise visualization of bending deformations of delaminated fragments. We deduce from these time deformations, a characteristic relaxation time which is recovered with indentation testing measurements. This duration stands for the relaxation time for the stress. In addition, different behaviors are evidenced during the delamination process: the system is elastic when delamination starts, then becomes plastic and viscoplastic. The experiments have been reproduced using four systems exhibiting different mechanical properties.

Table 1
Main characteristics for the samples considered in the experiments. Particle diameter: $2a$, solid weight fraction ϕ_m (data given by the manufacturer Grace Davison).

	$2a$ (nm)	ϕ_m
Ludox SM-30	10	0.30
Ludox HS-40	16	0.40
Ludox TM-50	26	0.50
nanolatex PS	30	0.30

2. Experimental

2.1. Starting materials

Four different types of particulate materials were used: concentrated aqueous dispersions of silica particles (Ludox SM-30, HS-40, TM-50 purchased from Sigma–Aldrich) and nanolatex particles (provided by Rhodia Recherche, Aubervilliers, France); HS-40 was used in most experiments. Main properties of these dispersions are reported in Table 1. These dispersions are stable in the absence of evaporation. In the case of the silica sols, the stability of the dispersion is governed by the interparticle colloidal interaction, e.g., by the competition between van der Waals attraction and electrostatic repulsion (Derjaguin–Landau–Verwey–Overbeek[7,8]). In the case of the nanolatex, particles are made of polystyrene, stabilized by the presence of surfactants (SDS); since the glass transition temperature of the particles is around 100 *dgrC*, the particles are assumed to be rigid (not deformable) at room temperature. Values of the surface tension $\gamma_{w,a}$ of the dispersions were measured by the Wilhelmy plate method and range in [57;67] mN m^{-1}. For each dispersion, the weak polydispersity of the particles prevents from crystallization (polydispersity ∼0.18).

2.2. Methods

The dynamics of delamination is investigated by observation of a strip of gel in side view. A sketch of the experimental set-up is shown in Fig. 2a. Experiments are performed by drawing a horizontal Nylon fiber, radius 200 μm, out of a fluid reservoir at a constant velocity. The reservoir contains the aqueous colloidal dispersion, and as the wire is pulling, a uniform film of constant thickness coats all around the fiber. Note that the characteristic time for the hydrodynamic instability, e.g. Rayleigh-Plateau instability growth rate, is larger than the characteristic time for drying [9]; it implies that no variations of the film thickness are detected before the material starts to consolidate. After the motor is stopped the film is let to dry at an ambient relative humidity RH ∼50%: particles concentrate and a gel of typical thickness 10 μm is formed. During the solidification

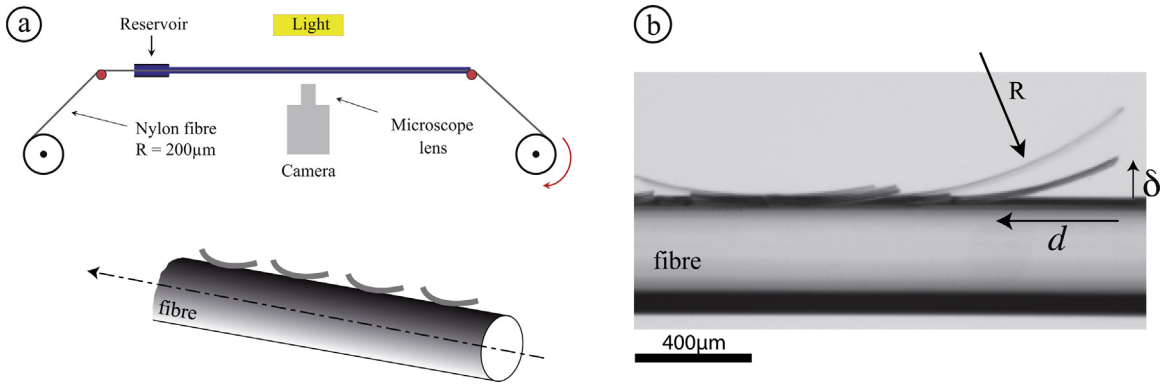

Fig. 2. (a) Sketch of a fiber passing through a colloidal dispersion reservoir. The fiber is coated evenly all around. Observation in side view uses a light transmission technique. (b) Colloidal films warped due to a moisture gradient upwards; typical size of the gelled strip is 20 µm wide and 10 µm thick.

of the films large stresses develop, resulting in annular cracks then transversal cracks parallel to the fiber-axis [10]. Further evaporation results in warping of a strip of gel at the upper line of the horizontal fiber (Fig. 2b). Observations use a light transmission technique; a microscope lens (15×) adapted to a camera (AVT's Marlin) provides digitized images with a resolution about 0.5 µm/pixel. The camera is mounted on a micrometric assembly allowing a precise alignment of the field of view with the film. This particular geometry provides accurately measurement of the peeling fragments with time. Further evaporation results in warping of fragments of gel. These delaminated fragments are observed all around the fiber but, the ones which are on the lower part of the fiber quickly fall out. We focus then on the upper part of the fiber as depicted in Fig. 2a; we follow the displacement of a delaminated fragment with time. We measure then the deflection δ and the interfacial crack advance d. We assume that the interfacial crack starts when the deformation of a fragment is of the order of a fraction of the film thickness.

3. Model

For all the experiments reported here, the film is made of a porous medium, fully saturated with water. The saturated system is then transparent because of the similarity in refractive index of the liquid and the solid. If air were present in the system, because of the lower value of index, there were significant scattering of light which implies the system to turn opaque. Thus, the cracks appear during the first stage of the drying process, e.g., the constant rate period where the decrease in volume material is equal to the volume of liquid lost by evaporation. The liquid/air meniscii are present at the evaporation surface; as a result the particles get closer and the local liquid pressure p in the pores, increases. It can reach a maximum value given by $P_{cap} = \alpha \frac{\gamma_{w,a}}{r'_p}$, where r'_p is the pore radius close to the particle radius a and α is a geometrical constant (<10)[11].

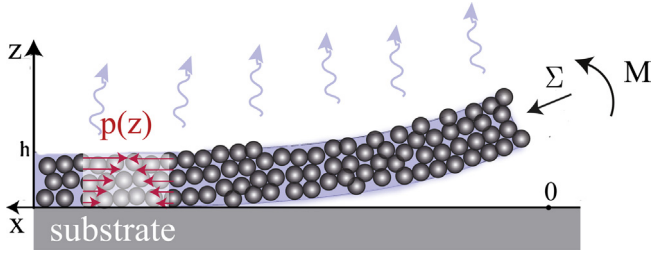

Fig. 3. Delamination of a drying film induced by differential stress in the porous film. The stress distribution induced by the pressure distribution, $p(z)$, results in an averaged force per unit depth, Σ, and a moment per unit depth, M, and causes the film to warp.

As a result the tension in the liquid pore compresses the matrix and induces flow from the bulk to the interface. It results in a pressure gradient in the pore liquid as depicted in Fig. 3: the spatial variation in pore pressure causes a variation in contraction of the gel network. The evaporation from the bottom side of a fragment is negligible as the air between the fiber and the film is saturated with water. Moreover the pore pressure is time dependent since it varies during the drying process.

Therefore the local liquid pressure p in the pores obeys a one-dimensional diffusion equation along the z vertical direction:

$$\frac{\partial p}{\partial t} = D_p \frac{\partial^2 p}{\partial z^2} \tag{1}$$

where $D_p = \frac{kE}{\eta}$ is the diffusivity, or consolidation coefficient, with E the elastic modulus of the gel, and η the viscosity of the solvent flowing through the porous gel of permeability k. We assume that the Young modulus is constant over the experiment time (about 200 s). A typical rigidity of the porous network, measured just after cracks formation, gives $E = 1 \pm 0.3$ GPa [10]. For randomly-packed monodisperse spheres k is given by the Carman–Kozeny relation: $k = \frac{1}{45} \frac{(1-\phi_g)^3}{\phi_g^2} a^2$, where ϕ_g is the particle volume fraction of the gel phase ($\phi_g \sim 0.6$) and $k = 2.3 \times 10^{-19} \mathrm{m}^2$. Moreover a steady rate of evaporation V_E is assumed at the upper surface of the gel $z = h$. The Darcy law gives the gradient of liquid pressure at the upper surface of the gel:

$$\frac{\partial p}{\partial z}|_{z=h} = -\frac{V_E \eta}{k} \tag{2}$$

Eq. (1) together with the boundary condition 2 give the pore pressure distribution $p(z, t)$ [11]. The stress distribution in the plane of the film, initially uniform without pressure gradient ($p(z, t = 0) = p_0$) under uniaxial strain and constant vertical stress (vertical stress is 0 and horizontal strains are 0), expresses as [12]:

$$\sigma(z, t) \propto p_0 - p(z, t) \tag{3}$$

Eqs. (1)–(3) show that the drying stress averaged on the film thickness linearly increases with time as:

$$\Sigma(t) \approx E V_E t \tag{4}$$

A delamination process occurs when the stored elastic strain energy overcomes the adhesion energy of the gel attached to the substrate. Experimental observations attest that the delamination process always starts from the edges of the fragments. The drying stress is then responsible for the development of a peel force per unit length, Σ, and consequently a bending moment $M(t) = \int_0^h (z - h/2)\sigma(z, t)dz$, per unit depth, that can lift the edges of the fragment and so generate convex surfaces [11,5] (see Fig. 3). The moment

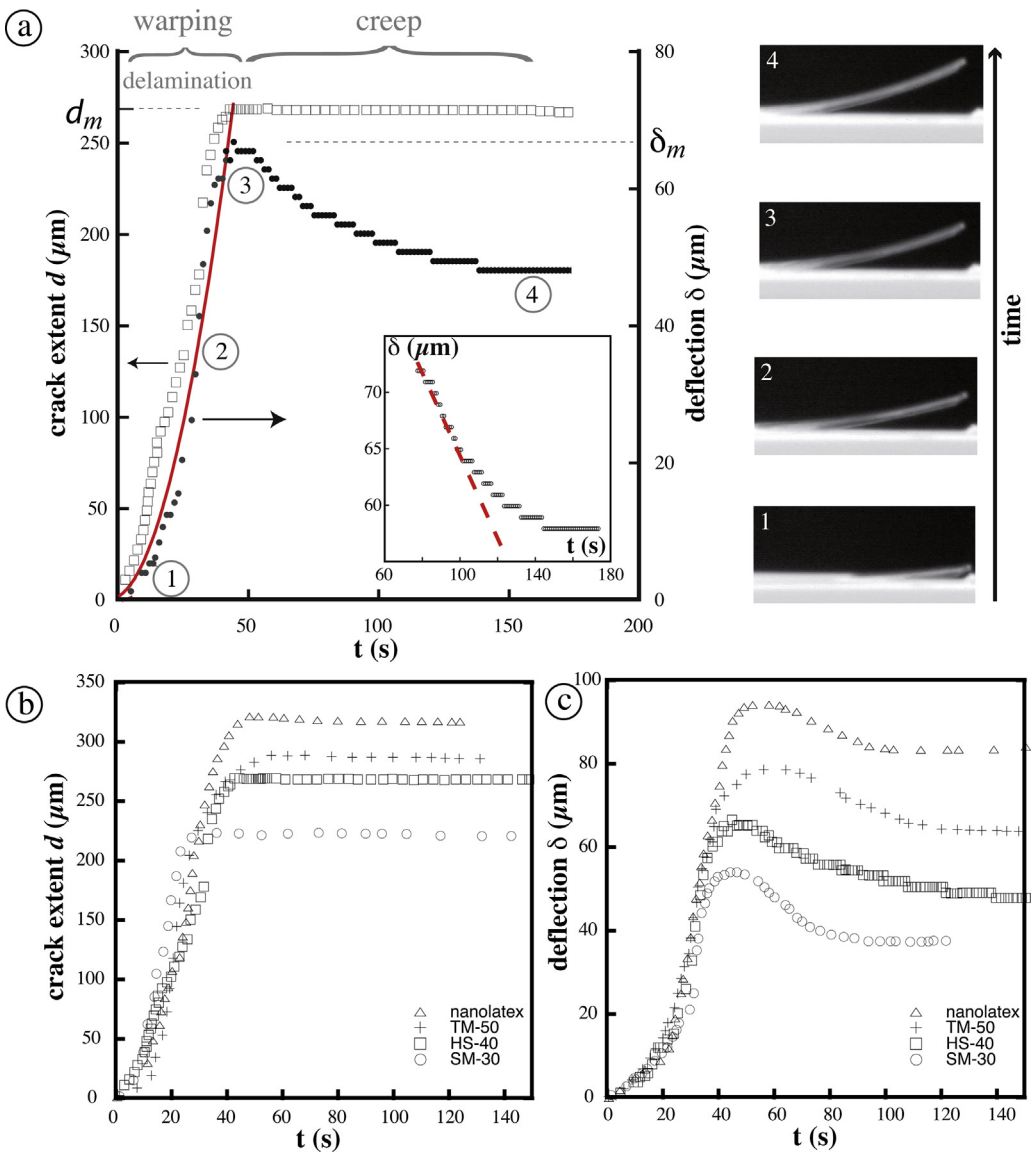

Fig. 4. (a) Time variation of the crack extent d and the deflection δ of a strip of gel (HS-40). The dynamics reveals different regimes: (1,2,3) elastic regime induced by warping where both the deflection and the crack extent increase (line is a fit of the deflection versus time using Eq. (5)); (4) then the deflection decreases as a signature of a creep behavior, while the crack extent d is constant. Inset shows a magnification of the time variation of the deflection in the creep regime. (b) Time variation of the crack extent for various colloidal films. (c) Time variation of the deflection for various colloidal films. (For interpretation of the references to color in the text of this figure citation, the reader is referred to the web version of this article.)

$M(t)$ is estimated by $M(t) \sim \Sigma(t)h$. The deflection δ of the warping fragment is related to the bending moment M by: $\frac{\partial^2 \delta}{\partial x^2} = \frac{M}{EI}$, where $I = \frac{1}{12}h^3$ is the moment of inertia [13] (Fig. 2b). Using Eqs. (1), (2) and (4), δ approximately expresses as:

$$\delta(t) \sim 12 \frac{V_E d(t)^2}{h^2} t \tag{5}$$

where $d(t)$ is the interfacial crack extent at time t.

This simple model provides an expression for δ as a function of time in the elastic regime.

4. Results and discussion

Experimentally, the dynamic of delamination can be characterized by the time evolution of two lengths: the deflection $\delta(t)$ which is the maximum height of the fragment lift at time t, and the interfacial crack extent $d(t)$ (see Fig. 2). During the gel warping, both the deflection δ and the crack extent d increase with time; the interfacial crack propagates quasi-statically in the x-direction. The time variation of the deflection is governed by the development of the drying stress and fairly satisfies Eq. (5) (red curve in Fig. 4). The gelled film exhibits an elastic behavior until the deflection reaches a maximum value δ_m. At this point, the drying stress reaches a maximum value related to the maximum capillary pressure generated by the fluid in a porous matrix: $\sigma(h, t_m) = -P_{cap}$. This quantity can be compared to the yield stress of the material suggesting that the material reaches a plastic behavior [14]. Then, in a second stage, since the strip of the gel still dries, the crack extent reaches a constant value, whereas, the deflection starts decreasing slowly to end up at a constant value as a result of a deformation due to sustained loading. The exponential-like decrease of the deflection δ evidences a creep behavior with a relaxation time t_r (see Fig. 4). t_r stands for the relaxation time of the stress in the strip gel due to sustained external capillary stress. The elastic modulus E_0 of a given particle (silica or latex at high glass transition temperature) is assumed of

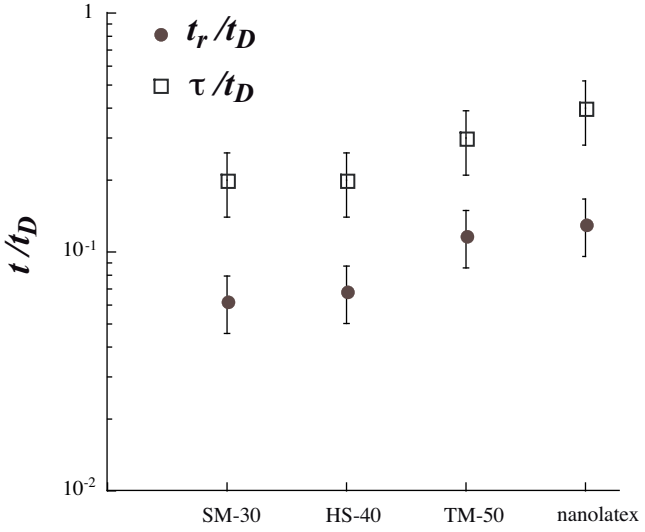

Fig. 5. Comparison of relaxation times in the creep regime for different systems; SM-30, HS-40, TM-50 and nanolatex in increasing order of rigidity. Time t_r is estimated by the slope of the deflection of the gel at the beginning of the creep regime (see inset in Fig. 4). Time $\tau = \frac{\eta_0}{E}$ is deduced from the fit of experimental results by the Kelvin–Voigt model (Eq. (6)). Time t_D is the characteristic drying time.

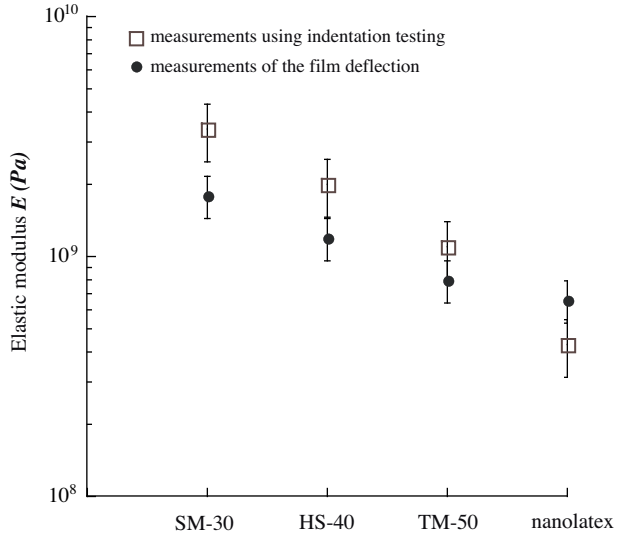

Fig. 7. Comparison of elastic moduli measured in the creep regime for different systems by two methods: (i) using indentation testing and modeling the solid layer by a Kelvin–Voigt model two-element model (a purely viscous damper of viscosity η_0 and a purely elastic spring connected in parallel, in accordance with Eq. (6)), and (ii) using measurements of the time relaxation t_r of the deflected strip of gel (the elastic modulus is then deduced from the quantity η_0/t_r). SM-30, HS-40, TM-50 and nanolatex in increasing order of rigidity.

the order of the elastic modulus of the drying gel under the condition of a cohesive network of particles. Since measurements using indentation testing provide typical values for silica and nanolatex gels of the order of 10^9 Pa, the strain due to the maximum stress, $\sigma_m \sim -P_{cap} = 10^7$ Pa, is of the order of to $10^{-2} \ll 1$. Thus we assumed that particles are not deformable due to capillary pressure.

Fig. 5 shows the ratio between t_r and the drying time $t_D = h/V_E$ for different systems, in increasing order of particle size from SM-30 to nanolatex. Results show the decrease of t_r with the size of the particles. A system made of small particles, is more rigid and the relaxation time for the stress increases.

To confirm and to complete these statements on the mechanical properties of the systems, we have performed indentation testing measurements. The method investigated here on the micron or sub-micron scale is indentation testing (CSM Instruments Micro Indentation testing, MHT) with a Rockwell indenter (0.25 mm radius spherical tip)[15]. The indenter, initially in contact with the surface of the solid film, is driven in the material until a maximal force $F_m = 70$ mN load with a loading speed 70 mN/min. The constant force is then maintained on the material (fragment of gel adhering on a glass substrate) and the penetration depth is measured as a function of time. The experiments have been performed on a layer of 10 μm just after cracks appear. Fig. 6 gives the evolution with time of the penetration depth for four systems. We use a Kelvin–Voigt model to fit the curves with a viscous and elastic component (a purely viscous damper and purely elastic spring

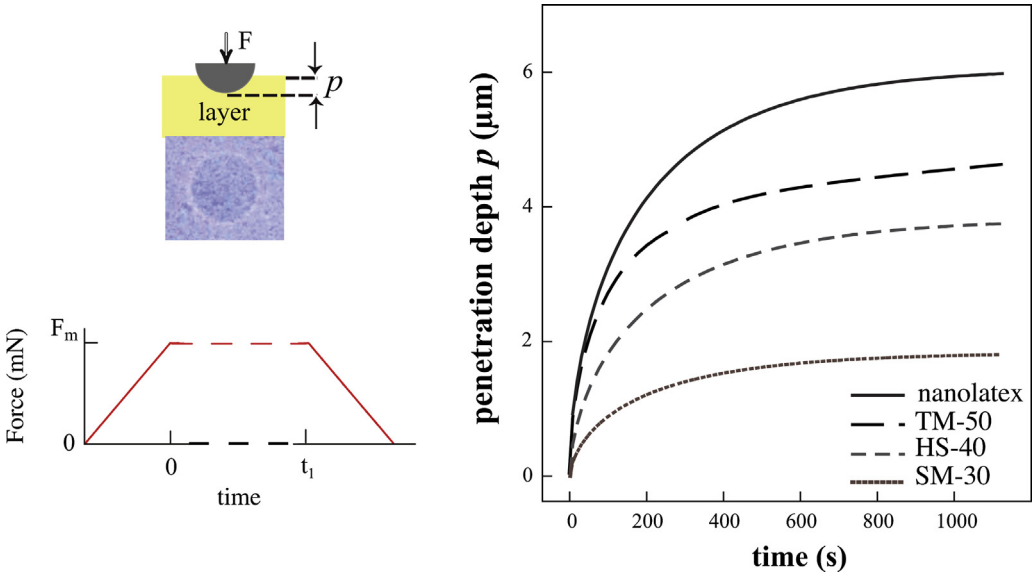

Fig. 6. Measurements of the macroscopic elastic response of the gel using indentation testing. Variation of the applied force F versus time (maximum load F_m: 70 mN); image of indentation print at the surface of the gel after unloading of a spherical indenter (Rockwell indenter of diameter 25 μm). Creep comparison of different colloidal films from 70 mN indents with 10 mN/min loading rate: the change in depth, p, of the indenter tip is measured as a function of time.

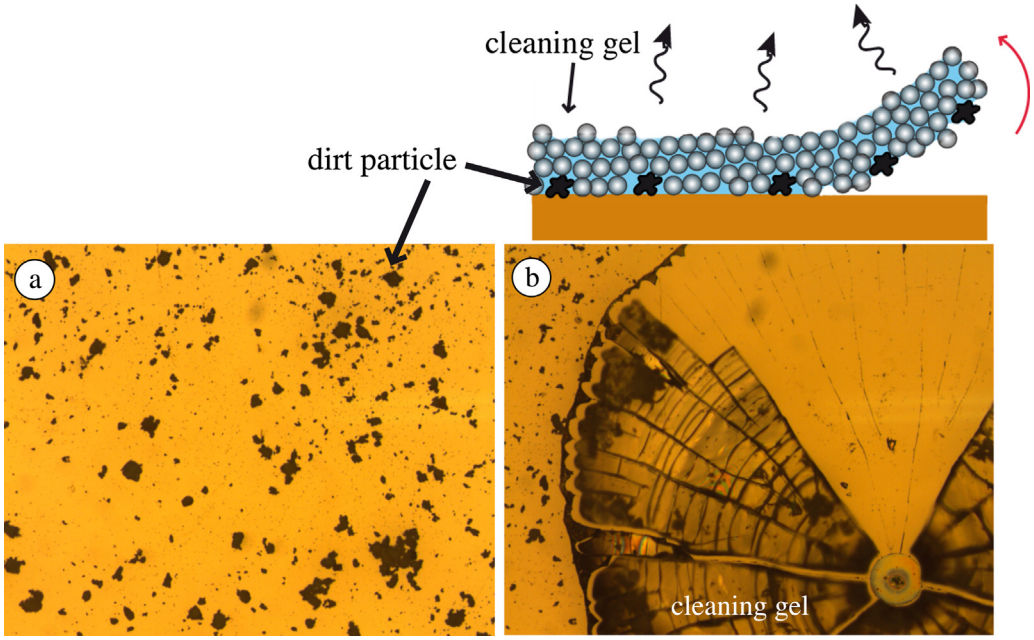

Fig. 8. (a) Dirt particles on a model glass slide. (b) Dirt particles have been removed after deposition of a colloidal film and delamination of the formed gel. Images width: 1 mm.

connected in parallel). The creep response to an external force F_m could be expressed as:

$$\delta^{3/2}(t) = \frac{3}{4\sqrt{r}} F_m \frac{1}{E}(1 - e^{(-\frac{E}{\eta_0}t)}) \quad (6)$$

where r is the spherical indenter radius, E and η_0 are fit parameters representing the elastic modulus of the material (corresponding to the spring element), and a viscosity term that quantifies the time dependent property of the material, respectively [16]. We assume that the elastic modulus is constant over the experiment time (about 200 s) [10].

By the way a timescale τ can be defined from creep tests as: $\tau = \frac{\eta_0}{E}$. This quantity corresponds physically to the timescale of the stress release in the material; the larger this relaxation time is, the longer the matrix can be reorganized to relax stresses. It then attestes of a creep behavior.

Fig. 5 shows a comparison between the time scale τ deduced from creep tests and the relaxation time t_r extracted from the deflection measurements. Both methods provide similar results for the studied systems; note that there is a constant delay between τ and t_r, and the evolution with the systems is the same.

Consequently, the elastic modulus measured in the creep regime can be deduced using the characteristic viscosity of the gel deduced from the Kelvin–Voigt model (Eq. (6)) and the timescale τ deduced from Eq. (6) or the timescale t_r of the deflected strip of gel (Fig. 4(a-inset)). Elastic moduli E are plotted in Fig. 7 for the different systems.

Both methods provide similar results, nevertheless, the results obtained with indentation testing are always higher than the ones obtained with the deflection.

5. Conclusion

Dynamic of delamination induced by warping of colloidal films is investigated using a one-dimensional geometry. This particular geometry allows us to image accurately the deflection of a strip of gel. As a result different mechanical behaviors can be pointed out during the drying process. The dynamic delamination highlights the combination of different mechanical features during the drying. Therefore, the out-of-plane displacement fairly satisfies a purely elastic behavior until it reaches a plastic one. Direct measurements, supported by indentation testing, allow us to estimate the elastic moduli of various colloidal gels, and the relaxation time of the stress for various colloidal gels. In particular, the rigidity of the materials increases with the particle size of the gel as predicted by the elastic modulus of an assembly of particles.

As a perspective on this work, the characterization of out-of-plane deformation of drying gels is based on an innovative process applied to cleaning surfaces. The first step of this process should be the deposition of a dispersion of nanoparticles on top of a substrate that one wishes cleaning. Then as water evaporates, the nanoparticles aggregate to form the porous gel network in which the dirt particles are included and trapped. Capillary forces will cause this gel to shrink and break into small solid pieces and finally delaminate from the substrate as illustrated in Fig. 8. The principle of this operation has been tested for the cleaning of surfaces that are contaminated by radioactive species [17]. The technique could be adapted to other substrates, particularly paintings to be restored.

Acknowledgements

We thank F. Boulogne and H. Laujay for fruitful discussions, and A. Aubertin, L. Auffray, and R. Pidoux for engineering and technical support.

References

[1] V. Lazarus, L. Pauchard, From craquelures to spiral crack patterns: influence of layer thickness on the crack patterns induced by desiccation, Soft Matter 7 (2011) 2552–2559.
[2] A. Groisman, E. Kaplan, An experimental study of cracking induced by desiccation, Europhys. Lett. 25 (1994) 415–420.
[3] A.F. Routh, Drying of thin colloidal films, Rep. Prog. Phys. 76 (2013) 046603.
[4] J.W. Hutchinson, Z. Suo, Mixed mode cracking in layered materials, Adv. Appl. Mech. 29 (1992) 63.
[5] R.W. Style, S.S.L. Peppin, A.C.F. Cocks, Mud peeling and horizontal crack formation in drying clays, J. Geophys. Res. 16 (2011) F01025.
[6] L. Pauchard, Patterns caused by buckle-driven delamination in desiccated colloidal gels, Europhys. Lett. 74 (2006) 188–1891.

[7] B.V. Derjaguin, L. Landau, Theory of the stability of strongly charged lyophobic sols and of the adhesion of strongly charged particles in solution of electrolytes, Acta Physicochim. URSS 14 (1941) 633.
[8] E.J.W. Verwey, J.T.G. Overbeek, Theory of Stability of Lyophilic Colloids, Elsevier, Amsterdam, 1948.
[9] F. Boulogne, L. Pauchard, F. Giorgiutti-Dauphiné, Effect of a non-volatile cosolvent on crack patterns induced by desiccation of a colloidal gel, Soft Matter 8 (2012) 8505.
[10] F. Boulogne, L. Pauchard, F. Giorgiutti-Dauphiné, Annular cracks in thin films of nanoparticle suspensions drying on a fiber, Europhys. Lett. 102 (2013) 39002.
[11] C.J. Brinker, G.W. Scherer, Sol–Gel Science: The Physics and Chemistry of Sol–Gel Processing, Elsevier Science, 1990.
[12] H.F. Wang, Theory of Linear Poroelasticity with Applications to Geomechanics and Hydrogeology, Princeton University Press, 2000.
[13] L.D. Landau, E.M. Lifshitz, Theory of Elasticity (Course of Theoretical Physics), vol. 7, Elsevier, 1986.
[14] L. Goehring, W.J. Clegg, A.F. Routh, Plasticity and fracture in drying colloidal films, Phys. Rev. Lett. 110 (2013) 024301.
[15] J. Malzbender, J.M.J. den Toonder, A.R. Balkenende, G. de With, Measuring mechanical properties of coatings: a methodology applied to nano-particle-filled sol–gel coatings on glass, Mater. Sci. Eng. R: Rep. 36 (2–3) (2002) 47–103.
[16] K.L. Johnson, Contact Mechanics, Cambridge University Press, 2001.
[17] F. Cuer and S. Faure. Biological decontamination gel, and method for decontaminating surfaces using said gel. World patent wo 12/001046, CEA Marcoule, 2012.